Sustainable and scalable *in-situ* synthesis of hydrochar-wrapped Ti_3AlC_2-derived nanofibers as adsorbents to remove heavy metals

Xinsheng Dong[a,b,c], Yaquan Wang[a,b,c], Mingmin Jia[a,b,c], Zhaoyang Niu[b], Junmeng Cai[d], Xi Yu[e], Xuebin Ke[f], Xingguang Zhang[a,b,c]* and Jianfeng Yao[a,b,c]*

Affiliations:

[a]Jiangsu Co-Innovation Center of Efficient Processing and Utilization of Forest Resources, Nanjing Forestry University, Nanjing, Jiangsu 210037, P. R. China.

[b]College of Chemical Engineering, Nanjing Forestry University, Nanjing, Jiangsu 210037, P. R. China. Email: x.g.zhang@njfu.edu.cn Email: jfyao@njfu.edu.cn

[c]Jiangsu Key Lab for the Chemistry & Utilization of Agricultural and Forest Biomass, Nanjing Forestry University, Nanjing, Jiangsu 210037, P. R. China.

[d]Biomass Energy Engineering Research Center, School of Agriculture and Biology, Shanghai Jiao Tong University, 800 Dongchuan Road, Shanghai 200240, P.R. China.

[e]European Bioenergy Research Institute (EBRI), Aston University, Birmingham B4 7ET, UK

[f]School of Engineering and Computer Science, University of Hull, HU6 7RX, UK.

Abstract:

To ensure a sustainable future, it is imperative to efficiently utilize abundant biomass to produce such as platform chemicals, transport fuels, and other raw materials; hydrochar is one

of the promising candidates derived by hydrothermal carbonization of biomass in pressurized hot water. The synthesis of "hydrochar-wrapped Ti_3AlC_2-derived nanofibers" was successfully achieved by a facile one-pot hydrothermal reaction using glucose as the hydrochar precursor. Meanwhile, cellulose and pinewood sawdust as raw materials were also investigated. Products were characterized by XRD, N_2 adsorption-desorption isotherms, SEM, TEM, FT-IR, and EDS to investigate their crystal structures, textural properties, morphologies, surface species and elemental compositions. In the adsorption test to remove Cd(II) and Cu(II) in aqueous solution, hydrochar-wrapped nanofibers outperformed pure nanofibers derived from Ti_3AlC_2, hydrothermal carbon derived from glucose and commercial activated carbon. Finally, the regeneration and sorption kinetics were also studied.

Keywords: Hydrochar, Ti_3AlC_2, adsorption; heavy metals.

Highlights

1. Hydrochar-wrapped nanofibers derived from Ti_3AlC_2 MAX phases were successfully prepared using glucose as a precursor.
2. Hydrochar-wrapped nanofibers exhibited higher adsorptive performances as to Cd(II) and Cu(II) compared with pure nanofibers derived from Ti_3AlC_2, hydrothermal carbon derived from glucose, and commercial activated carbon.
3. Using cellulose or pinewood sawdust as hydrochar precursors, adsorption capacities were also enhanced, offering a sustainable and scalable process to prepare high-performance adsorbents.

4. Adsorbents are prepared by fluoride-free hydrothermal reaction and fibrerous materials are easily recyclable.

1. Introduction

Rapid developments of industrialization and burgeoning increase in population have depleted nonrenewable resources and polluted natural environments. It is promising to ensure a sustainable future via efficient exploitation of abundant biomass to produce such as platform chemicals, transport fuels, and other raw materials.(Liu et al., 2015; Zhang et al., 2016b) Hydrochar is one of the promising candidates derived from hydrothermal carbonization of biomass in compressed hot water (130-250^{o}C). Compared with slow-pyrolysis of biomass at high temperatures (300-650^{o}C) to yield biochar, the hydrothermal carbonization process possesses advantages of cost-efficiency and convenience in direct utilization of wet feedstock without pre-drying requirement.(Kambo & Dutta, 2015) The hydrochar produced differs significantly from biochar in physiochemical properties that determine their potential applications in such as agriculture, energy production, environmental protection, catalysis and adsorption.(Deng et al., 2016; Fang et al., 2018)

The presence of heavy metals in water resources poses a detrimental effect on human beings and aquatic lives.(Qiu et al., 2018; Santhosh et al., 2016) For instance, copper ions once ingested excessively in the human diet may cause itching, dermatitis, vomiting, cramps, convulsions, and even death;(Hu et al., 2012) Cadmium (Cd) has been classified as a human carcinogen and teratogen impacting lungs, kidneys, liver and reproductive organs.(Waalkes, 2000) The remediation of polluted water remains a urgent issue particularly in underdeveloped countries, and measures of adsorption,(Sun et al., 2015; Wang et al., 2019; Wang et al., 2018b) chemical deposition,(Zou et al., 2016) electrodialysis,(Jiang et al., 2018) ion exchange,(Ciobanu

et al., 2015) solvent extraction,(van Osch et al., 2016) distillation,(Attia et al., 2018) ultra filtration,(Karim et al., 2016) and reverse osmosis(Akin et al., 2011) have been taken to remove heavy metals from wasted water. Among these methods, adsorption technology is inexpensive, easily scalable, and relatively environmental-friendly, and thus the activated carbon-based adsorbents are quite popular; however, activated carbon has limited adsorption capacity for heavy metal ions, owing to insufficient adsorptive sites.(Faur-Brasquet et al., 2002) In this regard, the aforementioned eco-friendly hydrochar is a promising substitute for their competency to capture heavy metals (e.g. Hg^{2+}, Cu^{2+}) in aqueous solution.(Saber et al., 2018; Wang et al., 2018a) Studies have demonstrated that hydrocar possesses abundant surface functional groups (e.g., COOH, OH, CO) to ensure remarkably enhanced adsorption capacity for heavy metals by electrostatic attraction, ion exchange, and surface complexation.(Mohan et al., 2014; Xu et al., 2008) Recently, composite adsorbents of attapulgite clay@carbon heterogeneous structures are prepared by a one-pot hydrothermal process, and outperform carbon-based materials to remove heavy metals of Cr(VI) and Pb(II).(Chen et al., 2011)

These studies inspire us to envisage that the Ti_3AlC_2 MAX phases should be an excellent candidate to combine with hydrochar because they have typical layered ternary metal carbides, nitrides, or carbonitrides(Lei et al., 2015) and can achieve functional surface species after treatment with exfoliation. Reports have focused on their electrical, thermal and mechanical properties(Sloof et al., 2016) and structural evolution into MXenes (e.g. Ti_3C_2, Ti_2C) and other nanomaterials(Ghidiu et al., 2014) or composites.(Rakhi et al., 2016) However, few studies systematically investigate its transformation to nanofiberous materials. This work develops a

scalable *in-situ* synthetic method to prepare "hydrochar-wrapped Ti_3AlC_2-derived nanofibers" (denoted as HCTNFs), utilizing glucose, cellulose or pinewood sawdust as the hydrochar precursors. To our best knowledge, there are no reports on the *in-situ* combination of TNFs with hydrochar as adsorbents for removal of heavy metals. The experimental results reveal that the bonded interfacial materials formed between hydrochar and nanofibers offers an intrinsically strong and stable structure. In the adsorption of Cu(II) and Cd(II), these new adsorbents outperform their counterparts of hydrothermal carbon derived from glucose, commercial activated carbon and pure nanofibers owing to the fully exposed surface oxygenated functionalities. These findings are encouraging and should spark intensive studies on utilizing biomass-based materials for other applications in such as catalysis, materials design and energy storage.(Cai et al., 2017; Deng et al., 2016; Zhang et al., 2016b)

2. Materials and methods

2.1 Chemicals

The following chemicals were purchased: Ti_3AlC_2 (~98% purity), NaOH (96%, Xilong Scientific Co., Ltd., China), $Cd(CH_3COO)_2{\cdot}2H_2O$ (chemical reagents, Sinopharm Chemical Reagent Co. Ltd., China), $CuSO_4{\cdot}5H_2O$ (99%, Shanghai Xinbao Fine Chemical Factory, China), $C_6H_{12}O_6{\cdot}H_2O$ (analytical reagents, Sinopharm Chemical Reagent Co.,Ltd., China), Microcrystalline cellulose (analytical reagents, Tianjin Guangfu Fine Chemical Research Institute, China), Sawdust (Liuan, Anhui, China).

2.2 Optimization of the synthesis of "Ti_3AlC_2-derived nanofibers"

The transformation of Ti_3AlC_2 MAX phases was according to the method reported in our

previous study.(Zhang et al., 2014) Typically, 3 g of the Ti_3AlC_2 particles were mixed with 40 mL of NaOH aqueous solution (10 mol/L) under stirring for 24 h at room temperature. After stirring, the suspension was transferred into a 100-mL autoclave with a PTFE container inside. The autoclave was maintained at temperature of 180°C for 48h in an oven under static conditions. Following hydrothermal treatment and cooling down to room temperature naturally, the solid products were recovered by filtration, washed with deionized water to remove excessive NaOH, until the pH = 7-9. Then the samples were dried at 60°C overnight without further treatment. Additionally, to optimize synthetic conditions, the concentration of NaOH aqueous solution, hydrothermal temperatures, and reaction time were systematically optimized. The "Ti_3AlC_2-derived nanofibers" were denoted as TNFs and the detailed experimental information and the associated characterization results were provided in the **Section 1**, **ESI**.

2.3 Synthesis of "hydrochar-wrapped Ti_3AlC_2-derived nanofibers"

The hydrothermal conditions to synthesize "hydrochar-wrapped Ti_3AlC_2-derived nanofibers" (HCTNFs) were performed under the aforementioned optimized experimental conditions, using three different precursors: glucose, cellulose, and pinewood sawdust. The Glu@TNFs was synthesized as the following procedures: 1 g of Ti_3AlC_2 MAX powder (200 mesh) was mixed with 15 mL of 10 mol L^{-1} NaOH solution. The suspension was continuously stirred for 3h at ambient conditions. 1, 2, or 4 g of glucose was mixed with the solution respectively and stirred for 1h. The solution was subsequently transferred into a 100-mL autoclave with a PTFE container inside. The autoclave was maintained at 180°C for 48 h under static conditions. The precipitate was recovered and washed with distilled water to remove

excessive NaOH, until the pH ranged from 7 to 9. Finally, the precipitate was washed with ethanol and then the obtained product was dried at 80 °C for 12 h. The samples prepared with different weight ratios of glucose/Ti_3AlC_2, and the products were denoted as Glu@TNFs-1, Glu@TNFs-2, Glu@TNFs-3. For comparison, 1 g of glucose was also hydrothermally treated under the same conditions, and the final product was denoted as hydrothermal carbon. The Cel@TNFs was synthesized by the same procedure as Glu@TNFs, except for the use of cellulose instead of glucose. 0.9, 1.8, or 3.6 g of cellulose was mixed with the solution and stirred for 1h. The samples prepared with different weight ratios of cellulose/Ti_3AlC_2 were denoted as Cel@TNFs-1, Cel@TNFs-2, Cel@TNFs-3. The Saw@TNFs was synthesized by the same procedure as Glu@TNFs, except using sawdust instead of glucose. 2, 4, or 8 g of sawdust was mixed with the solution and stirred for 1h. The samples prepared with different weight ratios of sawdust/Ti_3AlC_2 were denoted as Saw@TNFs-1, Saw@TNFs-2, Saw@TNFs-3. (Note: the amount of cellulose or sawdust added was according to the estimation that 1 g of glucose can be produced by hydrolyzing 0.9 g of cellulose or 2 g sawdust.(Asawaworarit et al., 2019; Yuan et al., 2019)

2.4 Characterizations

The crystal phases of samples were analyzed by X-ray diffraction (XRD) using Rigaku Smartlab with Cu Kα radiation (λ = 0.1542 nm) at a scan rate of 5°/min from 5 to 80 (2θ) at a voltage of 40 kV. Fourier transform infrared spectra (FTIR) was used to detect the surface functional groups by a FTIR spectrophotometer (Thermo Electron Nicolet-360, USA) using the KBr wafer technique 400-4000 cm^{-1}. The morphology of the samples was examined by

Field-emission scanning electron microscopy (FESEM) utilizing a JSM-7600F (JEOL Ltd., Japan) with an operating voltage of 30 kV. Transmission electron microscopy (TEM) images were obtained by a JEOL JEM-2100 instrument at the accelerating voltage of 200 kV. The compositions of the samples were analyzed by energy-dispersive X-ray spectroscopy (EDX) attached to the FESEM instrument. Five random spots have been performed to calculate the elemental composition. Zeta potentials were measured by the ZETASIZER Nano-ZS from Malvern Instruments with the liquid concentration of 0.75 mg/mL at initial pH value (~6). Nitrogen (N_2) adsorption-desorption analysis was conducted using the Micromeritics ASAP 2020 at 77 K. The specific surface areas were measured by the Brunauer-Emmett-Teller (BET) method. The concentration of Cd(II) and Cu(II) were determined by an atomic absorption spectrometer (PinAAcle 900F, American PerkinElmer).

2.5 Adsorptive capacity test

A stock solution of 100 mg L^{-1} Cd(II) or Cu(II) was prepared using $Cd(CH_3COO)_2 \cdot 2H_2O$ or $CuSO_4 \cdot 5H_2O$ in distilled water. The adsorption capacity of different composites was calculated according to the equation:

$$q_e = \frac{(C_0 - C_e)V}{m} \quad (1)$$

Where q_e (mg g^{-1}) is the adsorption capacity at equilibrium, C_0 (mg L^{-1}) is the initial concentration of Cu(II) or Cd(II) and C_e (mg L^{-1}) is the equilibrium concentration of Cu(II) or Cd(II); V (mL) and m (mg) represent the volume of the solution and the mass of the adsorbent, respectively.

The adsorption kinetics experiments were performed to evaluate the adsorption rates of

Cd(II) or Cu(II) on the representative adsorbent of Glu@TNFs-3, Cel@TNFs-3, and Saw@TNFs-3. The initial concentration of Cd(II) or Cu(II) was 100 mg L^{-1}. Typically, 15 mg of sample was added in 15 mL of the tested solution, and the suspension was stirred at room temperature for 24h to reach the equilibrium; then the concentration of metal ions was determined by an atomic absorption spectrometer. In order to further determine the contact time required to reach the equilibrium and to understand the rate of the sorption process, pseudo-first-order and pseudo-second-order were exploited to simulate the experimental data. The pseudo-first-order kinetic model and pseudo-second-order kinetic models are presented as follows:

$$\ln(q_e - q_t) = \ln q_e - k_1 t \quad (2)$$

$$\frac{t}{q_t} = \frac{1}{k_2 q_e^2} + \frac{t}{q_e} \quad (3)$$

Where q_e and q_t are the adsorption capacities (mg g^{-1}) at equilibrium time and at the time of t (min), respectively; k_1 (min^{-1}) and k_2 (g mg^{-1} min^{-1}) represent the rate constant of the pseudo-first-order and pseudo-second-order models, respectively.

3. Results and discussion

3.1 Characterization of "hydrochar-wrapped Ti_3AlC_2-derived nanofibers"

Figure 1

The crystallographic structures of the pristine Ti_3AlC_2, TNFs, Glu@TNFs-3, Cel@TNFs-3, Saw@TNFs-3, and hydrothermal carbon (derived from glucose) were characterized by XRD.

As shown in **Fig. 1a**, the diffraction peaks at 9.5°, 19.1°, 36.7°, 38.1°, 39°, 41.7°, 48.4° and 60.1°are assigned to the crystal facets of (002), (004), (101), (103), (008), (105), (107) and (110), corresponding to the typi1cal crystal phases of Ti_3AlC_2 (JCPDS no. 52-0875).(Kajiyama et al., 2016; Peng et al., 2014) After hydrothermal treatment of Ti_3AlC_2 by concentrated NaOH solution, Ti_3AlC_2 was transformed into nanosheets, nanofibers or bulk particles, essentially depending upon the hydrothermal conditions (e.g. concentrations of NaOH solution, hydrothermal temperatures, and reaction time; more information can be found in **Section 1**, **ESI**.) The crystal structure evolution, the morphological transformation, and the possible mechanism were also provided.).(Xie et al., 2014) In this work, the nanofibers were prepared under the optimized hydrothermal conditions (10 mol/L NaOH solution, 180^{o}C and 48h), they preserved the primary characteristic peaks of Ti_3AlC_2, and also showed newly-appeared peaks at the 2θ of 10.3^o, 25.0^o and 29.7^o. In contrast, the hydrothermal carbon derived from glucose exhibited no sharp peaks but a broad peak at 2θ angles of 10-30^o, which were attributed to the (002) plane of amorphous carbon, revealing that glucose had been carbonized.(Hara et al., 2004; Okamura et al., 2006) The Glu@TNFs-3 exhibited sharp peaks of TNFs with much lower intensities and broad peaks of amorphous carbon, demonstrating a composite structure of them. For Cel@TNFs-3 and Saw@TNFs-3, the characteristic peaks of TNFs was lower compared with those of pure TNFs, and the broad peaks of amorphous carbon were not as identifiable as those of Glu@TNFs-1, probably because the hydrochar formed was heterogeneously coated on the surface of TNFs (for comparison, all XRD patterns of Glu@TNFs, Cel@TNFs, and Saw@TNFs were provided in **Section 2**, **ESI**).

The N_2 adsorption-desorption isotherms of hydrothermal carbon, TNFs, Glu@TNFs-3, Cel@TNFs-3 and Saw@TNFs-3 are shown in **Fig. 1(b)**. The HCTNFs exhibit a typical type IV isotherm with a hysteresis loop attributable to the presence of the mesoporous structure in the HCTNFs;(Zhang et al., 2016a) In addition, the hysteresis loops formed between 0.8-1.0 (P/P_0) are mainly due to the formation of inter-particle avoids. According to BET measurements, the specific surface areas are obtained as the following: hydrothermal carbon (19.4 m^2 g^{-1}), TNFs (1.0 m^2 g^{-1}), Glu@TNFs-3 (37.0 m^2 g^{-1}), Cel@TNFs-3 (38.9 m^2 g^{-1}), and Saw@TNFs-3 (16.2 m^2 g^{-1}) (The BET surface areas of all Glu@TNFs, Cel@TNFs and Saw@TNFs can be found in the **Section 3**, **ESI**, and the N_2 adsorption-desorption isotherms of these aforementioned samples were given in **Section 4**, **ESI**). The specific surface areas of HCTNFs nanofibers were much higher than that of pristine Ti_3AlC_2 powder (1.2 m^2 g^{-1}) and the urchin-like rutile titania carbon composites of e-TACFs and e-TACSs (16.4 m^2 g^{-1} and 1.6 m^2 g^{-1}).(Gu et al., 2018; Sun et al., 2009; Xie et al., 2014) The BET surface area of the Glu@TNFs-3 (37.0 m^2 g^{-1}) is approximately 30 times that of the etched TNFs (1.2 m^2 g^{-1}), and is approximately 2 times higher than that of Saw@TNFs-3 (16.2 m^2 g^{-1}).

Figure 2

To investigate the morphological transformation, SEM and TEM images were collected. In detail, SEM images of Glu@TNFs-3 are displayed in **Fig. 2(a)**, the morphologies of Ti_3AlC_2 MAX phases are transformed from particles to nanofibers after etching. Compared with TNFs

(**Fig. s2d**), Glu@TNFs-3 is fully wrapped by homogeneous hydrochar derived from glucose, and the surfaces possessed oxygen-containing functional groups.(Fard et al., 2017) SEM images of Cel@TNFs-3 are displayed in **Fig. 2(b)**, similarly, the morphologies are transformed from bulk particles (MAX phases) to nanofibers. Cel@TNFs-3 is coated by hydrochar derived from cellulose and big hydrocar particles formed at higher content of cellulose because of the hydrogen bond connections. SEM images of Saw@TNFs-3 are illustrated in **Fig. 2(c)**, the morphology is transformed from particles (MAX phases) to nanofibers. Sawdust was slowly dissolved in NaOH solution and formed thick hydrochar layers. To confirm the structures between hydrochar and TNFs, TEM characterizations were performed and the TEM images are given in **Fig. 2(d-f)**. The hydrochar wrapped structures of Glu@TNFs-3 are successfully constructed, the width of Glu@TNFs is between 10 nm and 50 nm, and the width of nanofibers is mainly concentrated around 20 nm. When cellulose was used, hydrochar-coated Ti_3AlC_2 nanofibers formed, having different diameters of 10 nm to 80 nm. As to Saw@TNFs, the diameters of nanofibers vary from 20 nm to 80 nm. All these results demonstrate that hydrochar-wrapped structures can be potentially optimized as to the char precursors and synthetic conditions.

Additionally, the chemical composition of these HCTNFs was evaluated by SEM-EDX elemental analysis (detailed results can be found in **Table S1, Section 3, ESI**). The NaOH etching removed Al elements and its content was lower than 4 at.% in the HCTNFs, but the Al content is 17 at.% in parent Ti_3AlC_2 phase.

3.2 Adsorption capacity studies

Figure 3

The adsorption capacities of HCTNFs are displayed in **Section 5**, **ESI** and typical samples of Glu@TNFs-3, Cel@TNFs-3, and Saw@TNFs-3 were shown in **Fig. 3**. As to the adsorption of Cd(II), the HCTNFs exhibited much better adsorptive performances than those of Ti_3AlC_2, TNFs, hydrothermal carbon and commercial activated carbon, thus demonstrating that the distributed hydrochar on nanofibers outperformed hydrochar big particles derived from glucose. The Glu@TNFs-2 and Cel@TNFs-3 showed similar adsorptive performances as Cd(II), slightly better than Saw@TNFs-3 did. The change in precursor amount of glucose, cellulose, or sawdust added did not show an obvious improving trend of adsorptive performances. For Cu(II), it is obvious that more hydrochar precursors added resulted in higher the adsorption capacities of HCTNFs: Glu@TNFs was from 29.0 mg g^{-1} to 38.3 mg g^{-1}; Cel@TNFs was from 35.9 mg g^{-1} to 41.6 mg g^{-1}; Saw@TNFs was from 32.1 mg g^{-1} to 40.0 mg g^{-1}. Generally, the adsorption capacities of HCTNFs were much higher than those of Ti_3AlC_2, TNFs, hydrothermal carbon and commercial activated carbon, probably because of the abundant oxygen-containing functional groups on their surface and this will be discussed later on in the proposed mechanism.(Elaigwu et al., 2014; Fuertes et al., 2010; Liu et al., 2010) Moreover, HCTNFs exhibited a higher adsorption capacity than many other materials reported in literature (detailed information was provided in **Table s2-s3** in **Section 6**, **ESI**).

3.3 Regeneration of adsorbents and sorption kinetics

To test the reusability of these adsorbents, the regeneration experiments were performed for 8 h by adding spent Glu@TNFs-3 in 30 mL of 0.2 mol L^{-1} HCl solution under stirring to remove Cd(II). After regeneration, the adsorption capacity of Glu@TNFs-3 was 61.1mg g^{-1}, which proved that Glu@TNFs-3 had strong reusability.

Figure 4

Sorption kinetics were investigated to calculate the adsorption rate of Cd(II) and Cu(II) on Glu@TNFs-3, Cel@TNFs-3 and Saw@TNFs-3. **Fig. 4** shows the adsorption curves of Cd(II) and Cu(II) on Glu@TNFs-3, Cel@TNFs-3, and Saw@TNFs-3 under different contact time periods. Results of sorption kinetics demonstrate that Cd(II) and Cu(II) uptake is a two distinct stage adsorption process. The rapid adsorption of Cd(II) and Cu(II) can be achieved within 10 min, and then a slow sorption stage is found for approaching equilibrium within 120 min for Cd(II) and 360 min for Cu(II). The rapid adsorption stage can be ascribed to abundant fresh functional groups on their surfaces, and then the surfaces are gradually occupied by Cd(II) or Cu(II) ions, which lead to a plodding adsorption stage.

The k_1 and q_e values of the pseudo-first-order model were obtained from the linear plot of $\ln(q_e - q_t)$ versus t (min) (figure not shown). Meanwhile, the plot of t/q versus t (min) was linearly fitted to calculate the pseudo-second-order correlation parameters (**Fig. s8a-f**, **Section 7**, **ESI**). According to the correlation coefficients (R^2) (given in **Table s4-s5**, **Section 7**, **ESI**) it can be concluded that the pseudo-second-order model fitted the kinetic data better than the

pseudo-first-order model did. Moreover, the k_2 of Cu(II) adsorption on Saw@TNFs-3 was 6.5 × 10^{-3} g mg^{-1} min^{-1}, which was much higher than that on Glu@TNFs-3 and Cel@TNFs-3 (k_2 = 3.8 × 10^{-3} g mg^{-1} min^{-1}), indicating that the adsorption rate of Cu(II) on Saw@TNFs-3 was faster than that of Cu(II) on Glu@TNFs-3 and Cel@TNFs-3. The k_2 of Cd(II) adsorption on Glu@TNFs-3 was 4.2 × 10^{-3} g mg^{-1} min^{-1}, which was much higher than that on Cel@TNFs-3 (k_2 = 1.6 × 10^{-3} g mg^{-1} min^{-1}) and Saw@TNFs-3 (k_2 = 1.3 × 10^{-3} g mg^{-1} min^{-1}). This phenomenon further revealed that the rate-determining mechanism for Cd(II) and Cu(II) adsorption on Glu@TNFs-3, Cel@TNFs-3, and Saw@TNFs-3 was the chemisorption. Therefore, hydrochar-coated TNFs with more exposed surface functional adsorptive sites could adsorb these heavy metals faster than pure TNFs, hydrothermal carbon, and commercial activated carbon.

3.4. Mechanistic discussion

The experimental results of HCTNFs preparation demonstrated that hydrochar precursors of glucose, which completely dissolved in the synthetic solution, could form coherent and homogeneous hydro-wrapped structures due to the hydrogen-bonded interfacial materials between hydrochar and TNFs. On the contrary, cellulose and sawdust underwent hydrolysis first and then hydrogen-bonded with TNFs, this slow process gave rise to heterogeneously distributed hydrochar particles on TNFs.

As to the adsorptive capacity, zeta potential and FT-IR analyses were used to seek for the underlying reasons. As a representative, the zeta potential of Glu@TNFs-3 was -10.9 mV at a pH=6, which can explain the efficient attraction of Cd(II) or Cu(II) owing to the electrostatic

attraction as a driving force.(Gu et al., 2018) In addition, the numerous oxygen-containing functional groups are reported to be a main reason for heavy metal adsorption by HCTNFs,(Kołodyńska et al., 2017) and the supported hydrochar on TNFs exposed more adsorptive sites than hydrothermal carbon, thereby performing better in the test adsorption of Cd(II) and Cu(II).

4. Conclusions

"Hydrochar-wrapped Ti_3AlC_2-derived nanofibers" (HCTNFs) were successfully prepared using glucose as the precursor; cellulose and pinewood sawdust were also investigated as precursors. HCTNFs had a higher adsorption capacity than pure nanofiber of TNFs, hydrothermal carbon and commercial activated carbon in the removal of heavy metals from water. The reasons for the enhanced adsorption ability are correlated to the interfacial materials between hydrochar and TNFs which offer more surface functional groups and also exhibited strong interactions with heavy metals. The method is distinguishing because it is fluoride-free and scalable, also controllable as to the product morphology and adsorptive capacity.

Acknowledgements：

The authors thank the National Natural Science Foundation of China (NNSFC21706134), the Young Natural Science Foundation of Jiangsu Province (BK20170918), and Natural Science Key Project of the Jiangsu Higher Education Institutions (15KJA220001) for financial support. Thank the technical support from the "Advanced analysis and testing center of Nanjing Forestry University".

References

Akin, I., Arslan, G., Tor, A., Cengeloglu, Y., Ersoz, M. 2011. Removal of arsenate [As(V)] and arsenite [As(III)] from water by SWHR and BW-30 reverse osmosis. *Desalination*, **281**, 88-92.

Asawaworarit, P., Daorattanachai, P., Laosiripojana, W., Sakdaronnarong, C., Shotipruk, A., Laosiripojana, N. 2019. Catalytic depolymerization of organosolv lignin from bagasse by carbonaceous solid acids derived from hydrothermal of lignocellulosic compounds. *Chemical Engineering Journal*, **356**, 461-471.

Attia, H., Johnson, D.J., Wright, C.J., Hilal, N. 2018. Comparison between dual-layer (superhydrophobic–hydrophobic) and single superhydrophobic layer electrospun membranes for heavy metal recovery by air-gap membrane distillation. *Desalination*, **439**, 31-45.

Cai, J., He, Y., Yu, X., Banks, S.W., Yang, Y., Zhang, X., Yu, Y., Liu, R., Bridgwater, A.V. 2017. Review of physicochemical properties and analytical characterization of lignocellulosic biomass. *Renewable and Sustainable Energy Reviews*, **76**, 309-322.

Chen, L.F., Liang, H.W., Lu, Y., Cui, C.H., Yu, S.H. 2011. Synthesis of an attapulgite clay@carbon nanocomposite adsorbent by a hydrothermal carbonization process and their application in the removal of toxic metal ions from water. *Langmuir*, **27**(14), 8998-9004.

Ciobanu, I., Josceanu, A., Guran, C., Minca, I. 2015. *Ion Chromatographic Method for Determination of Heavy Metals in Water*.

Deng, J., Li, M., Wang, Y. 2016. Biomass-derived carbon: synthesis and applications in energy storage and conversion. *Green Chemistry*, **18**(18), 4824-4854.

Elaigwu, S.E., Rocher, V., Kyriakou, G., Greenway, G.M. 2014. Removal of Pb^{2+} and Cd^{2+}

from aqueous solution using chars from pyrolysis and microwave-assisted hydrothermal carbonization of Prosopis africana shell. *Journal of Industrial and Engineering Chemistry*, **20**(5), 3467-3473.

Fang, J., Zhan, L., Ok, Y.S., Gao, B. 2018. Minireview of potential applications of hydrochar derived from hydrothermal carbonization of biomass. *Journal of Industrial and Engineering Chemistry*, **57**, 15-21.

Fard, A.K., McKay, G., Chamoun, R., Rhadfi, T., Preud'Homme, H., Atieh, M.A. 2017. Barium removal from synthetic natural and produced water using MXene as two dimensional (2-D) nanosheet adsorbent. *Chemical Engineering Journal*, **317**, 331-342.

Faur-Brasquet, C., Kadirvelu, K., Le Cloirec, P. 2002. Removal of metal ions from aqueous solution by adsorption onto activated carbon cloths: adsorption competition with organic matter. *Carbon*, **40**(13), 2387-2392.

Fuertes, A.B., Arbestain, M.C., Sevilla, M., Maciá-Agulló, J.A., Fiol, S., López, R., Smernik, R.J., Aitkenhead, W.P., Arce, F., Macías, F. 2010. Chemical and structural properties of carbonaceous products obtained by pyrolysis and hydrothermal carbonisation of corn stover. *Soil Research*, **48**(7), 618-626.

Ghidiu, M., Lukatskaya, M.R., Zhao, M.-Q., Gogotsi, Y., Barsoum, M.W. 2014. Conductive two-dimensional titanium carbide 'clay' with high volumetric capacitance. *Nature*, **516**, 78.

Gu, P., Xing, J., Wen, T., Zhang, R., Wang, J., Zhao, G., Hayat, T., Ai, Y., Lin, Z., Wang, X. 2018. Experimental and theoretical calculation investigation on efficient Pb(II) adsorption on

etched Ti_3AlC_2 nanofibers and nanosheets. *Environmental Science: Nano*, **5**(4), 946-955.

Hara, M., Yoshida, T., Takagaki, A., Takata, T., Kondo, J.N., Hayashi, S., Domen, K. 2004. A carbon material as a strong protonic acid. *Angew Chem Int Ed Engl*, **43**(22), 2955-8.

Hu, J., Yang, S., Wang, X. 2012. Adsorption of Cu(II) on β-cyclodextrin modified multiwall carbon nanotube/iron oxides in the absence/presence of fulvic acid. *Journal of Chemical Technology & Biotechnology*, **87**(5), 673-681.

Jiang, C., Chen, H., Zhang, Y., Feng, H., Shehzad, M.A., Wang, Y., Xu, T. 2018. Complexation Electrodialysis as a general method to simultaneously treat wastewaters with metal and organic matter. *Chemical Engineering Journal*, **348**, 952-959.

Kajiyama, S., Szabova, L., Sodeyama, K., Iinuma, H., Morita, R., Gotoh, K., Tateyama, Y., Okubo, M., Yamada, A. 2016. Sodium-Ion Intercalation Mechanism in MXene Nanosheets. *ACS Nano*, **10**(3), 3334-41.

Kambo, H.S., Dutta, A. 2015. A comparative review of biochar and hydrochar in terms of production, physico-chemical properties and applications. *Renewable and Sustainable Energy Reviews*, **45**, 359-378.

Karim, Z., Claudpierre, S., Grahn, M., Oksman, K., Mathew, A.P. 2016. Nanocellulose based functional membranes for water cleaning: Tailoring of mechanical properties, porosity and metal ion capture. *Journal of Membrane Science*, **514**, 418-428.

Kołodyńska, D., Krukowska, J., Thomas, P. 2017. Comparison of sorption and desorption studies of heavy metal ions from biochar and commercial active carbon. *Chemical Engineering Journal*, **307**, 353-363.

Lei, J.-C., Zhang, X., Zhou, Z. 2015. Recent advances in MXene: Preparation, properties, and applications. *Frontiers of Physics*, **10**(3), 276-286.

Liu, W.J., Jiang, H., Yu, H.Q. 2015. Development of Biochar-Based Functional Materials: Toward a Sustainable Platform Carbon Material. *Chem Rev*, **115**(22), 12251-85.

Liu, Z., Zhang, F.-S., Wu, J. 2010. Characterization and application of chars produced from pinewood pyrolysis and hydrothermal treatment. *Fuel*, **89**(2), 510-514.

Mohan, D., Sarswat, A., Ok, Y.S., Pittman, C.U. 2014. Organic and inorganic contaminants removal from water with biochar, a renewable, low cost and sustainable adsorbent – A critical review. *Bioresource Technology*, **160**, 191-202.

Okamura, M., Takagaki, A., Toda, M., Kondo, J.N., Domen, K., Tatsumi, T., Hara, M., Hayashi, S. 2006. Acid-Catalyzed Reactions on Flexible Polycyclic Aromatic Carbon in Amorphous Carbon. *Chemistry of Materials*, **18**(13), 3039-3045.

Peng, Q., Guo, J., Zhang, Q., Xiang, J., Liu, B., Zhou, A., Liu, R., Tian, Y. 2014. Unique lead adsorption behavior of activated hydroxyl group in two-dimensional titanium carbide. *J Am Chem Soc*, **136**(11), 4113-6.

Qiu, J., Zhang, X.-F., Zhang, X., Feng, Y., Li, Y., Yang, L., Lu, H., Yao, J. 2018. Constructing $Cd_{0.5}Zn_{0.5}S$@ZIF-8 nanocomposites through self-assembly strategy to enhance Cr(VI) photocatalytic reduction. *Journal of Hazardous Materials*, **349**, 234-241.

Rakhi, R.B., Nayak, P., Xia, C., Alshareef, H.N. 2016. Erratum: Novel amperometric glucose biosensor based on MXene nanocomposite. *Scientific Reports*, **6**, 38465.

Saber, M., Takahashi, F., Yoshikawa, K. 2018. Characterization and application of

microalgae hydrochar as a low-cost adsorbent for Cu(II) ion removal from aqueous solutions. *Environmental Science and Pollution Research*, **25**(32), 32721-32734.

Santhosh, C., Velmurugan, V., Jacob, G., Jeong, S.K., Grace, A.N., Bhatnagar, A. 2016. Role of nanomaterials in water treatment applications: A review. *Chemical Engineering Journal*, **306**, 1116-1137.

Sloof, W.G., Pei, R., McDonald, S.A., Fife, J.L., Shen, L., Boatemaa, L., Farle, A.-S., Yan, K., Zhang, X., van der Zwaag, S., Lee, P.D., Withers, P.J. 2016. Repeated crack healing in MAX-phase ceramics revealed by 4D in situ synchrotron X-ray tomographic microscopy. *Scientific Reports*, **6**, 23040.

Sun, Y., Yang, S., Chen, Y., Ding, C., Cheng, W., Wang, X. 2015. Adsorption and desorption of U(VI) on functionalized graphene oxides: a combined experimental and theoretical study. *Environ Sci Technol*, **49**(7), 4255-62.

Sun, Z., Li, M., Hu, L., Lu, X., Zhou, Y. 2009. Surface Chemistry, Dispersion Behavior, and Slip Casting of Ti_3AlC_2Suspensions. *Journal of the American Ceramic Society*, **92**(8), 1695-1702.

van Osch, D.J., Parmentier, D., Dietz, C.H., van den Bruinhorst, A., Tuinier, R., Kroon, M.C. 2016. Removal of alkali and transition metal ions from water with hydrophobic deep eutectic solvents. *Chem Commun (Camb)*, **52**(80), 11987-11990.

Waalkes, M.P. 2000. Cadmium carcinogenesis in review. *Journal of inorganic biochemistry*, **79**(1-4), 241-4.

Wang, H., Liu, Y., Ifthikar, J., Shi, L., Khan, A., Chen, Z., Chen, Z. 2018a. Towards a better

understanding on mercury adsorption by magnetic bio-adsorbents with γ-Fe_2O_3 from pinewood sawdust derived hydrochar: Influence of atmosphere in heat treatment. *Bioresource Technology*, **256**, 269-276.

Wang, Y., Feng, Y., Yao, J. 2019. Construction of hydrophobic alginate-based foams induced by zirconium ions for oil and organic solvent cleanup. *J Colloid Interface Sci*, **533**, 182-189.

Wang, Y., Feng, Y., Zhang, X.F., Zhang, X., Jiang, J., Yao, J. 2018b. Alginate-based attapulgite foams as efficient and recyclable adsorbents for the removal of heavy metals. *J Colloid Interface Sci*, **514**, 190-198.

Xie, X., Xue, Y., Li, L., Chen, S., Nie, Y., Ding, W., Wei, Z. 2014. Surface Al leached Ti_3AlC_2 as a substitute for carbon for use as a catalyst support in a harsh corrosive electrochemical system. *Nanoscale*, **6**(19), 11035-40.

Xu, Y.-J., Weinberg, G., Liu, X., Timpe, O., Schlögl, R., Su, D.S. 2008. Nanoarchitecturing of Activated Carbon: Facile Strategy for Chemical Functionalization of the Surface of Activated Carbon. *Advanced Functional Materials*, **18**(22), 3613-3619.

Yuan, S., Li, T., Wang, Y., Cai, B., Wen, X., Shen, S., Peng, X., Li, Y. 2019. Double-adsorption functional carbon based solid acids derived from copyrolysis of PVC and PE for cellulose hydrolysis. *Fuel*, **237**, 895-902.

Zhang, X., Durndell, L.J., Isaacs, M.A., Parlett, C.M.A., Lee, A.F., Wilson, K. 2016a. Platinum-Catalyzed Aqueous-Phase Hydrogenation of d-Glucose to d-Sorbitol. *ACS Catalysis*, **6**(11), 7409-7417.

Zhang, X., Ke, X., Zheng, Z., Liu, H., Zhu, H. 2014. TiO_2 nanofibers of different crystal phases for transesterification of alcohols with dimethyl carbonate. *Applied Catalysis B: Environmental*, **150-151**, 330-337.

Zhang, X., Wilson, K., Lee, A.F. 2016b. Heterogeneously Catalyzed Hydrothermal Processing of C5-C6 Sugars. *Chem Rev*, **116**(19), 12328-12368.

Zou, G., Guo, J., Peng, Q., Zhou, A., Zhang, Q., Liu, B. 2016. Synthesis of urchin-like rutile titania carbon nanocomposites by iron-facilitated phase transformation of MXene for environmental remediation. *Journal of Materials Chemistry A*, **4**(2), 489-499.

Figure captions

Fig. 1. XRD patterns (a) and N_2 adsorption–desorption isotherms (b) of the parent Ti_2AlC_3, TNFs, Glu@TNFs-3, Cel@TNFs-3, Saw@TNFs-3, and Hydrothermal carbon. Synthetic conditions: 10 mol/L NaOH aqueous solution, 180°C, 48h

Fig. 2. SEM images of Glu@TNFs-3 (a), Cel@TNFs-3 (b), and Saw@TNFs-3 (c); and TEM image of Glu@TNFs-3 (d) , Cel@TNFs-3 (e), and Saw@TNFs-3 (f). Synthetic conditions: 10 mol/L NaOH aqueous solution, 180°C, 48h

Fig. 3. Adsorption capacities of Ti_3AlC_2, TNFs, hydrothermal carbon, activated carbon and typical HCTNFs for Cu(II) and Cd(II). Conditions: pH(Cd) = 6, pH(Cu) = 5, $C(Cd)_{initial}$ = 100 mg L^{-1}, $C(Cu)_{initial}$ = 100 mg L^{-1}, m/V =1 g L^{-1} and T = 25°C.

Fig. 4. Effect of contact time on the adsorption capacities of Glu@TNFs-3, Cel@TNFs-3, and Saw@TNFs-3 for Cd(II) **(Left)** and Cu(II) **(Right)**. Test conditions: pH(Cd) = 6, pH(Cu) = 5, $C(Cd)_{initial}$ = 100 mg L^{-1}, $C(Cu)_{initial}$ = 100 mg L^{-1}, m/V =1 g L^{-1} and T = 298 K.

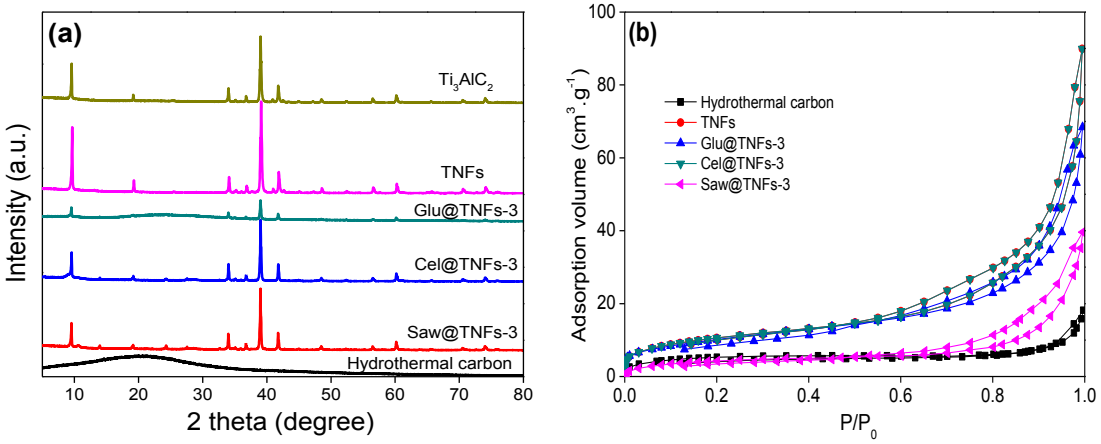
(a)
Ti3AlC2
TNFs
Glu@TNFs-3
Cel@TNFs-3
Saw@TNFs-3
Hydrothermal carbon
Intensity (a.u.)
10
20
30
40
50
60
70
80
2 theta (degree)
(b)
Hydrothermal carbon
TNFs
Glu@TNFs-3
Cel@TNFs-3
Saw@TNFs-3
Adsorption volume (cm3.g-1)
0
20
40
60
80
100
0.0
0.2
0.4
0.6
0.8
1.0
P/P0

Fig. 3

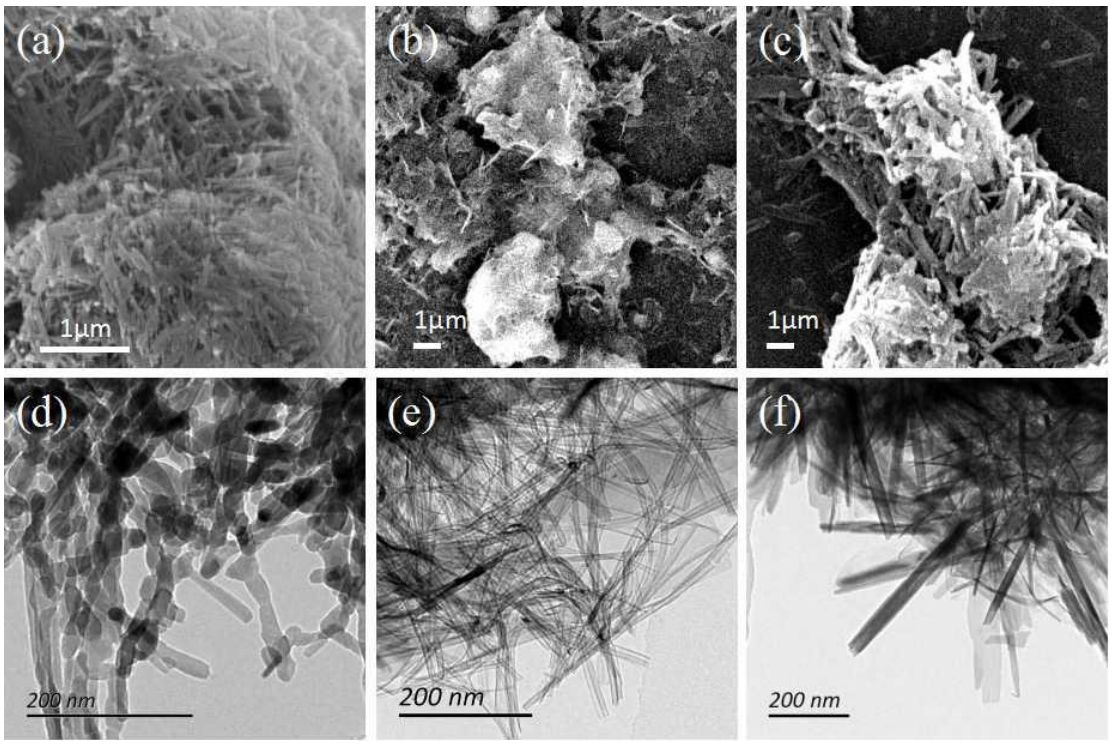
(a)
1μm
(b)
1μm
(c)
1μm
(d)
200 nm
(e)
200 nm
(f)
200 nm

Fig. 4

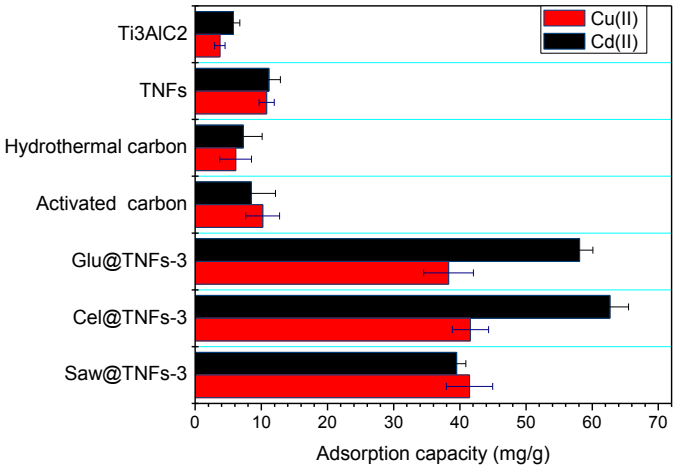
Ti3AlC2
TNFs
Hydrothermal carbon
Activated carbon
Glu@TNFs-3
Cel@TNFs-3
Saw@TNFs-3
Cu(II)
Cd(II)
0
10
20
30
40
50
60
70
Adsorption capacity (mg/g)

Fig. 3

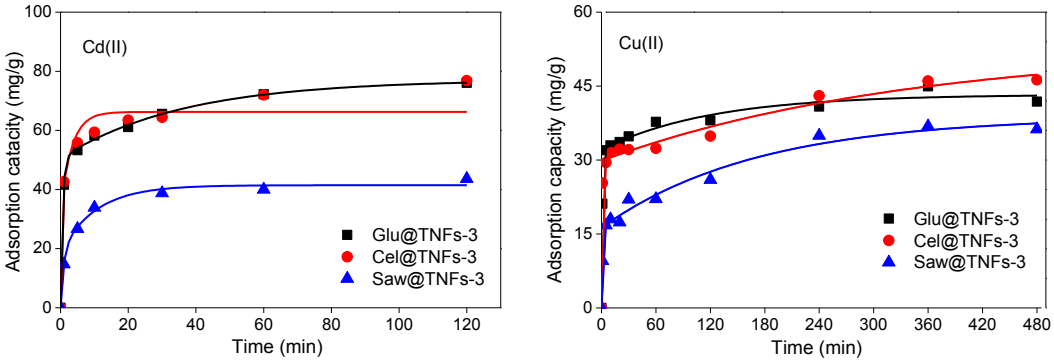
Cd(II)
Adsorption catacity (mg/g)
Time (min)
Glu@TNFs-3
Cel@TNFs-3
Saw@TNFs-3
Cu(II)
Adsorption capacity (mg/g)
Time (min)
Glu@TNFs-3
Cel@TNFs-3
Saw@TNFs-3

Fig. 4